

Two-dimensional numerical modeling of dam-break flow using a new TVD finite-element scheme

Omid Seyedashraf¹ · Ali Akbar Akhtari² 

Received: 12 November 2016 / Accepted: 25 March 2017 / Published online: 5 April 2017
© The Brazilian Society of Mechanical Sciences and Engineering 2017

Abstract A new numerical scheme based on the finite-element method with a total-variation-diminishing property is developed with the aim of studying the shock-capturing capability of the combination. The proposed model is formulated within the framework of the one-step Taylor–Galerkin scheme in conjunction with the Van Leer’s limiter function. The approach is applied to the two-dimensional shallow water equations by different test cases, i.e., the partial, circular, and one-dimensional dam-break flow problems. For the one-dimensional case, the sub- and supercritical flow regimes are considered. The results are compared with the analytical, finite-difference, and smoothed particle hydrodynamics solutions in the literature. The findings show that the proposed model can effectively mask the sources of errors in the abrupt changes of the flow conditions and is able to resolve the shock and rarefaction waves where other numerical models produce spurious oscillations.

Keywords Taylor–Galerkin method · Total-variation-diminishing · Shallow water equations · Dam-break flow

List of symbols

$B(r)$ Van Leer’s limiter
 d Constant coefficient
 F Flux vectors’ matrix
 g Gravity

G Flux vectors’ matrix
 h Water depth
 h_e Element size
 h_L Water depth in the upstream channel
 h_R Water depth in the downstream channel
 h_i Numerical depth results in each node
 i Node number
 K Stiffness matrix
 L Length of the computational domain
 M Mass matrix
 n Manning’s roughness coefficient
 S Topographical and frictional source terms
 S_{bx} Depth gradients in the x -directions
 S_{by} Depth gradients in the y -directions
 S_{fx} Friction slopes along x -directions
 S_{fy} Friction slopes along y -directions
 s Bore speed
 t Time
 U Matrix of variables
 u Depth-integrated velocity in the x -directions
 v Depth-integrated velocity in the y -directions
 x x -direction space
 y y -direction space
 Ψ_i Basis-function

1 Introduction

In numerical analysis, dam-break is the immediate release of an initially stationary water body by removing a vertical obstacle. When a dam is broken, flash flooding occurs as the impounded water flees through the opening in the downstream river. The dynamics of dam-break shock waves is rather complex, and its behavior does not meet the terms of the conventional assumptions of the steady

Technical Editor: Jader Barbosa Jr.

✉ Ali Akbar Akhtari
akhtari@razi.ac.ir

¹ Department of Civil Engineering, Kermanshah University of Technology, 6715685420 Kermanshah, Iran

² Department of Civil Engineering, Razi University, 6714967346 Kermanshah, Iran

and gradually varied open-channel flows. This fact is probably the major factor in the lag of investigations of dam-break flows compared to other free surface problems. The difficulty is to choose an appropriate technique for capturing the abrupt changes in the bore formation and flow velocity values while the wave propagates. To comply with these constraints, the employed numerical model must be founded on advanced techniques that inherent non-oscillatory advection [1].

In recent years, developing shock-capturing models has been the center of attention for engineers. There is a significant amount of literature dedicated to the satisfactory solutions of the shallow water equations for shock-dominated problems. These include the finite-difference method (FDM) [2–5], finite-volume method (FVM) [6, 7], finite-element method (FEM) [8–11], and smoothed hydrodynamic particle (SPH) models [12, 13]. For example, Zhang et al. [14] developed a hydrodynamic and sediment transport model for dam-break flow simulation using an explicit FVM based on the shallow water equation (SWE) system. FEM has also been effectively applied to similar flow problems [15, 16]. An attentive historical report of FEMs in this context is reported by Wang et al. [17] employing the Galerkin scheme to solve wave equations. Wang et al. [17] showed that the classic FEM is more efficient than the ordinary FDMs due to its rigorous mathematical theory and efficiency of creating complex geometries. Moreover, isogeometric analysis (IA) is superior to the SPH models for the imposition of boundary conditions [5]. However, Wang et al.'s [17] study was conducted using classic techniques, which results in fluctuations in the sharp discontinuities.

Accordingly, employing advanced numerical methods with the shock-capturing ability was inevitable. These techniques were later implemented by researchers such as Sheu and Fang [18] who merged the FEM and flux-corrected transport (FCT) methods and applied it to the SWEs. Later, Ortiz [9] also developed a finite-element model based on the FCT technique for shallow water flows to predict the evolution of coastlines.

The total-variation-diminishing (TVD) model is another shock-capturing scheme, which was initiated by Harten [19] to describe oscillations in the calculated results. The scheme was employed by Wang et al. [20] through a second-order Lax–Wendroff method in conjunction with an FDM to discretize the two-dimensional SWEs. More recently, Boulahia et al. [21] employed a similar TVD scheme for the numerical simulation of a one-dimensional flow for an inert gas mixture. Many other relevant works on applying this technique to the engineering applications of shock-dominated flow problems have been published [3, 22–24]. However, no work has been reported so far on

a combination of the FEM and TVD models to investigate the engineering problems with abrupt changes in the results, especially for the SWEs. Most of these studies are limited to the implementation of the TVD scheme along with the FDMs. Accordingly, this study proposes a finite-element model founded in the TVD concept based on Van Leer's flux-limiter. Here, the basal idea of the TVD method is to correct the algorithms with large oscillation errors in the water elevation, and velocity fields with anti-oscillation contributions using a local criterion to flag and correct the nodes for the maximum and minimum fluxes. The simulations are conducted in two-dimensional domains to demonstrate the features of the developed scheme. Here the topographic effects are ignored to simplify the validation process of the model. The accuracy of the obtained results is compared against the pre-existing analytical and numerical results as a validation process to the model [25, 26].

The rest of this paper is organized as follows. In Sect. 2, the governing equation system is presented and discussed. Section 3 describes the developed numerical procedure. In Sect. 4, four regularly used benchmarks are considered and employed to validate the developed model. Finally, Sect. 5 summarizes the findings of the study.

2 Mathematical theory

SWEs are typically derived by depth averaging the Navier–Stokes equations under the hydrostatic and Boussinesq approximations. Here, the resulting system yields the two-dimensional SWEs.

$$U_t + F_x + G_y + S = 0 \quad (1)$$

in which U represents the solution vector of conservative variables, F and G denote the flux vectors; S accounts for the topographical and frictional source terms, and the subscripts t , x and y represent the partial derivatives of the time and space, respectively.

$$U = \begin{Bmatrix} h \\ uh \\ vh \end{Bmatrix} \quad (2)$$

$$F = \begin{Bmatrix} uh \\ u^2h + gh^2/2 \\ uvh \end{Bmatrix} \quad (3)$$

$$G = \begin{Bmatrix} vh \\ uvh \\ v^2h + gh^2/2 \end{Bmatrix} \quad (4)$$

$$S = \left\{ \begin{array}{l} 0 \\ gh(S_{bx} - S_{fx}) \\ gh(S_{by} - S_{fy}) \end{array} \right\}, \tag{5}$$

where u and v are the depth-integrated velocity components in the x - and y -directions; respectively. g is gravity, h denotes the water depth, S_{bx} and S_{by} are defined by the depth gradients while S_{fx} and S_{fy} correspond to the friction slopes along the x - and y -directions, respectively.

$$S_{fx} = \frac{n^2 u(u^2 + v^2)^{1/2}}{h^{4/3}} \tag{6}$$

$$S_{fy} = \frac{n^2 v(u^2 + v^2)^{1/2}}{h^{4/3}}, \tag{7}$$

where n denotes Manning’s roughness coefficient.

To simplify the validation process, the homogeneous case is considered [25].

$$U_t + AU_x + BU_y = 0 \tag{8}$$

in which

$$A = \frac{dF(U)}{dU} = \begin{bmatrix} 0 & 1 & 0 \\ -u^2 + c^2 & 2u & 0 \\ -uv & v & u \end{bmatrix} \tag{9}$$

$$B = \frac{dG(U)}{dU} = \begin{bmatrix} 0 & 0 & 1 \\ -uv & v & u \\ -v^2 + c^2 & 0 & 2v \end{bmatrix}, \tag{10}$$

where

$$c = \sqrt{gh}. \tag{11}$$

3 Numerical scheme and resolution techniques

The process is the standard scientific approach to the computational fluid dynamics. The scheme is first order in space and second-order in time. In a view to discretize the governing equations in time, the following Taylor series expansion in its weak form was used in the time increment Δt [27].

$$\int_{\Omega} \psi_i \Delta U d\Omega = -\Delta t \left[\int_{\Omega} \psi_i \left(\frac{\partial F}{\partial x} \Big| ^n + \frac{\partial G}{\partial y} \Big| ^n \right) d\Omega \right] + \frac{\Delta t^2}{2} \left\{ \int_{\Omega} \psi_i \frac{\partial}{\partial x} \left[A^n \left(\frac{\partial F}{\partial x} \Big| ^n + \frac{\partial G}{\partial y} \Big| ^n \right) \right] d\Omega + \int_{\Omega} \psi_i \frac{\partial}{\partial y} \left[B^n \left(\frac{\partial F}{\partial x} \Big| ^n + \frac{\partial G}{\partial y} \Big| ^n \right) \right] d\Omega \right\} \tag{12}$$

in which ψ_i is the set of basis functions.

Conducting the Taylor series expansion of the fluxes, and combining the expressions into the second-order time derivative:

$$\frac{\partial^2 U}{\partial t^2} \Big| ^n = \frac{\partial}{\partial t} \frac{\partial U}{\partial t} = -\frac{\partial}{\partial t} \left(\frac{\partial F}{\partial x} + \frac{\partial G}{\partial y} \right)^n = -\frac{2}{\Delta t} \left[\frac{\partial}{\partial x} (F^{n+1/2} - F^n) + \frac{\partial}{\partial y} (G^{n+1/2} - G^n) \right] \tag{13}$$

Here, applying the Gauss theorem to the weak form of Eq. (8) yields:

$$\int_{\Omega} \psi_i U^{n+1} d\Omega = \int_{\Omega} \psi_i U^n d\Omega + \Delta t \left[\int_{\Omega} \frac{\partial}{\partial x} \psi_i F^{n+1/2} d\Omega + \int_{\Omega} \frac{\partial}{\partial y} \psi_i G^{n+1/2} d\Omega + \int_{\Gamma} \psi_i \frac{\partial}{\partial n} F^{n+1/2} d\Gamma + \int_{\Omega} \psi_i \frac{\partial}{\partial n} G^{n+1/2} d\Gamma \right] \tag{14}$$

This equation was discretized in space using the Bubnov–Galerkin method. However, the solution may suffer from spurious oscillations in the results near the sharp changes in the flow conditions. The strategy is to add a new term to the system functioning as a flux-limiter [28]:

$$\int_{\Omega} \psi_i U_i^{n+1} d\Omega = \int_{\Omega} \psi_i U_i^n d\Omega + RH_i^n + \sum_k d_{ik} K_{ik} (U_k^n - U_i^n), \tag{15}$$

where d is a coefficient, which is varied within the range [0, 1], and $K_{ij} = \sum_l \int_{T_l} \psi_i \psi_j d\Omega$. RH is the combination of the integral terms of the weak form equations’ right-hand side terms.

3.1 Flux-limiter

The second-order TVD scheme was obtained here through identifying the location of the probable oscillations and inserting a new term to reduce the dissipation. In a two-dimensional case, using the extrapolated points $\{i^*\}$ and $\{k^*\}$, the following variations were produced for each segment [29]:

$$\Delta_{i^*} q = q_i - q_{i^*}; \quad \Delta_{ik} q = q_k - q_i; \quad \Delta_{k^*} q = q_{k^*} - q_k, \tag{16}$$

where q_i is the unknown parameter. $q_{i^*} = q_k - 2 \vec{\nabla} q_i \cdot \vec{\eta}$ and $q_{k^*} = q_i + 2 \vec{\nabla} q_k \cdot \vec{\eta}$ are the extrapolated unknowns in direction $\vec{\eta} = (x_k - x_i; y_k - y_i)$. Moreover, d_{ik} is defined as follows:

$$d_{ik} = \begin{cases} 0 & \text{if } r^+ < 0 \text{ or } r^- < 0 \text{ (extremum)} \\ 1 - B(r_s^+, r_s^-) & \text{otherwise} \end{cases} \quad (17)$$

where

$$r^+ = \frac{\min(|\Delta_{k*}q|, |\Delta_{ik}q|)}{\max(|\Delta_{k*}q|, |\Delta_{ik}q|)}; \quad r^- = \frac{\min(|\Delta_{i*}q|, |\Delta_{ik}q|)}{\max(|\Delta_{i*}q|, |\Delta_{ik}q|)} \quad (18)$$

$$B(r_s^+, r_s^-) = \min[B(r_s^+), B(r_s^-)] \quad (19)$$

in which $B(r)$ is Van Leer’s limiter, which varies within the range $[0, 1]$:

$$B(r) = \min\left(\frac{2r}{1+r}, 1\right) \quad (20)$$

The dissipation coefficient was identical throughout the governing equations, while water depth was the main variable to obtain the sensor. Moreover, due to the explicit nature of the calculations, the Courant–Friedrichs–Lewy (CFL) criterion was honored as the stability condition [30]. According to this criterion, the time step Δt fulfill the following inequality:

$$CFL = \frac{\Delta t}{h_e} \left| \left(c + \sqrt{u^2 + v^2} \right) \right|_{\max} \leq 1, \quad (21)$$

where h_e is the element size.

4 Results and discussion

The developed TVD Taylor–Galerkin (TVD-TG) model was applied to four typical test cases, namely the one-dimensional dam-break considering both the sub- and supercritical flows, and the asymmetric and circular dam-break problems. The MATLAB software was devised to code the numerical procedure. Two constant relative water depths were defined as the Dirichlet boundary condition at the inlet and outlet sets. All other boundaries are defined as solid walls and described by a combination of Dirichlet and

Neumann boundary conditions by the integrations in the weak form of the equations.

4.1 One-dimensional dam-break problem (subcritical flow)

In this benchmark, the assumption of the immediate and complete dam break is considered, which is suitable for a reinforced concrete arch dam. The test demonstrates the flow field at $t = 36$ s. The computational domain is a 2000×200 m² horizontal and rectangular channel discretized by 2000 linear triangular elements. The chosen time step for the time discretization is $\Delta t = 0.39$ s. The dam is located in the middle of a horizontal channel, and the water body is assumed stationary with unequal depths on both sides of the dam (Fig. 1). The normal velocities along the boundary are assumed zero.

Figure 2 depicts the finite-element grid form of the computational domain.

The subcritical and supercritical flow regimes were obtained by changing the up- to downstream water depth ratios. For example, $\frac{h_0}{h_1} = \frac{5}{10}$ denotes the subcritical flow regime while $\frac{h_0}{h_1} = \frac{1}{10}$ represents a supercritical flow. The obtained results were compared with Stoker’s [25] analytical solution, obtained by solving the following polynomial equations.

$$u(x, t) = \begin{cases} 0 & \text{if } x < \frac{L}{2} - t\sqrt{gh_L} \\ \frac{1}{3t} (2(x + t\sqrt{gh_L}) - L) & \text{if } \frac{L}{2} - t\sqrt{gh_L} \leq x \leq (u_2 - c_2)t + \frac{L}{2} \\ u_2 & \text{if } (u_2 - c_2)t + \frac{L}{2} < x \leq st + \frac{L}{2} \\ 0 & \text{if } x > st + \frac{L}{2} \end{cases} \quad (22)$$

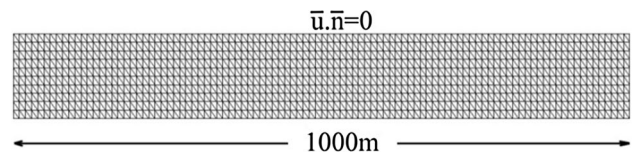
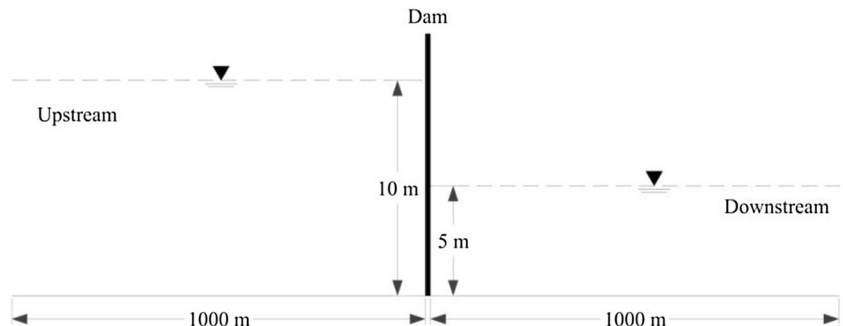


Fig. 2 The employed grid form

Fig. 1 Initial conditions for the dam-break problem



$$h(x, t) = \begin{cases} h_L & \text{if } x < \frac{L}{2} - t\sqrt{gh_L} \\ \frac{1}{9g} \left(2\sqrt{gh_L} - \frac{1}{2t}(2x - L) \right)^2 & \text{if } \frac{L}{2} - t\sqrt{gh_L} \leq x \leq (u_2 - c_2)t + \frac{L}{2} \\ \frac{h_R}{2} \left(\sqrt{1 + \frac{8s^2}{gh_R}} - 1 \right) & \text{if } (u_2 - c_2)t + \frac{L}{2} < x \leq st + \frac{L}{2} \\ h_R & \text{if } x > st + \frac{L}{2} \end{cases}, \tag{23}$$

where

$$u_2 = S - \frac{gh_R}{4S} \left(1 + \sqrt{1 + \frac{8s^2}{gh_R}} \right) \tag{24}$$

$$c_2 = \sqrt{\frac{gh_R}{2} \left(\sqrt{1 + \frac{8s^2}{gh_R}} - 1 \right)} \tag{25}$$

in which s is the positive root of $(u_2 + 2c_2 - 2\sqrt{gh_L})$, where L is the length of the domain, h_L is water depth on the left-hand side of the dam, and h_R denotes the water depth in the downstream channel.

To demonstrate the model’s efficiency, the results were also compared with two ideal FDM solutions regularly used for dam-break modeling. Accordingly, considering the same initial and boundary conditions, the SWEs were solved by the Lax–Wendroff and MacCormack procedures (Figs. 3, 4). All computations, including the numerical and analytical solutions, were performed in MATLAB 7.0.4.

Figures 3 and 4 show that the proposed TVD model produces the best fitting results comparing with the analytic solution. Moreover, it can be seen that the developed model is successful in predicting the formation of the shock and rarefaction waves without showing spurious fluctuations.

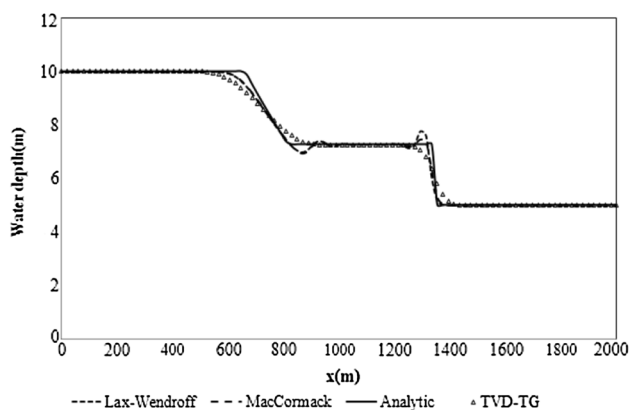


Fig. 3 One-dimensional dam-break flow problem ($h_1 = 10$ m, $h_0 = 5$ m and $t = 36$ s)

4.2 One-dimensional dam-break problem (supercritical flow)

Accurate simulation of supercritical flows is often complicated. Most of the numerical models introduced in the literature suffer from severe fluctuations in the abrupt changes of the flow conditions [13, 31, 32]. In this section, the capability of the developed model is assessed and compared to the analytical, FDM, and Chang et al.’s [13] SPH models. Figure 5 demonstrates the solution of a supercritical flow induced by dam-break, where the water depth ratio is 0.1.

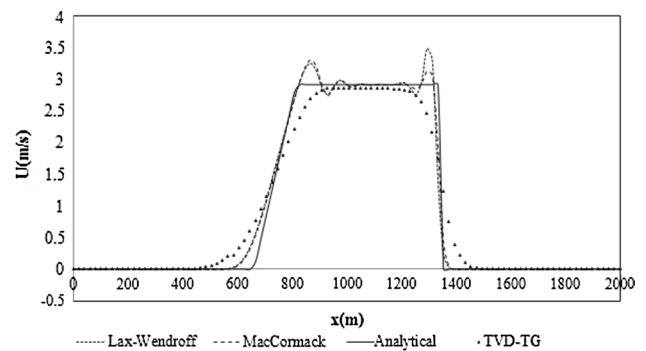


Fig. 4 Flow velocity results for the analytical and numerical simulation of the one-dimensional dam-break problem ($h_1 = 10$ m, $h_0 = 5$ m and $t = 36$ s)

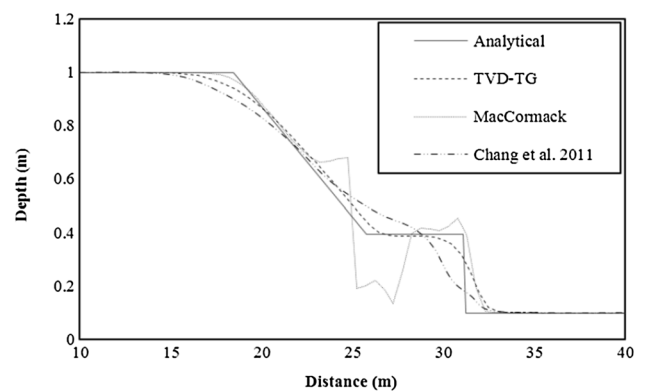


Fig. 5 Dam-break flow water depth results of the analytical solution with the current model, MacCormack, and the results of Chang et al. [13]

It can be seen that there is a deformation in the waveform in the MacCormack predictions. Moreover, the SPH model was not able to capture the shock formation. However, the developed model produces acceptable results.

4.3 Partial dam-break problem

The purpose of this benchmark is to evaluate the capability of the TVD-TG model to resolve the two-dimensional

wave propagation. There is no analytical solution to this problem. However, its numerical solutions are available in the literature [33–36]. Figure 6 depicts the geometric dimensions of the computational domain used for the flow simulation. Initially, the upstream discharge is assumed zero while the water depths are 10 m in the upstream, and 5 m in the downstream sections. The domain dimension is $200 \times 200 \text{ m}^2$, divided by 3200 triangular elements.

After the removal of the barrier, water sets free to flow through the downstream channel reach. The shock and rarefaction waves are formed in the domain propagating in reverse directions. Figure 7 demonstrates the water

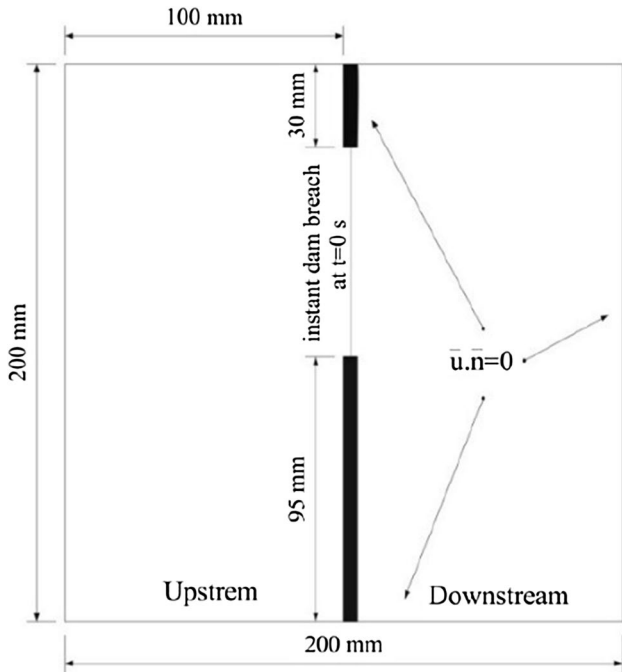


Fig. 6 The geometry of the partial dam-break problem

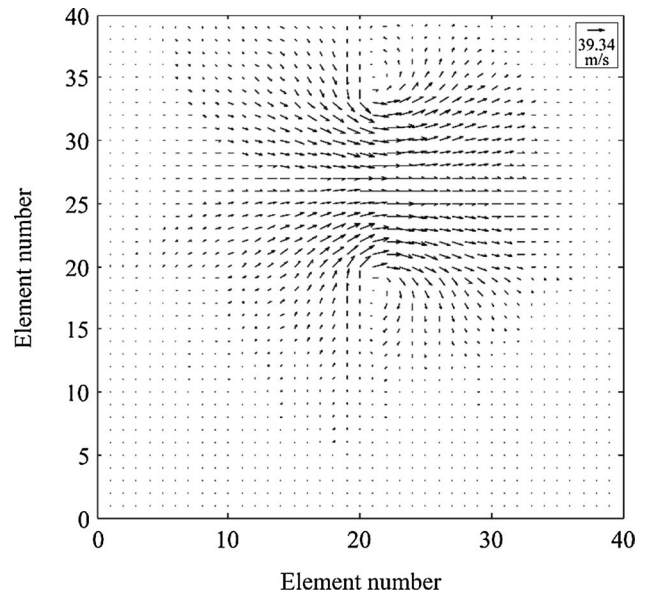


Fig. 8 The partial dam-break problem. Velocity field at $t = 7.2 \text{ s}$

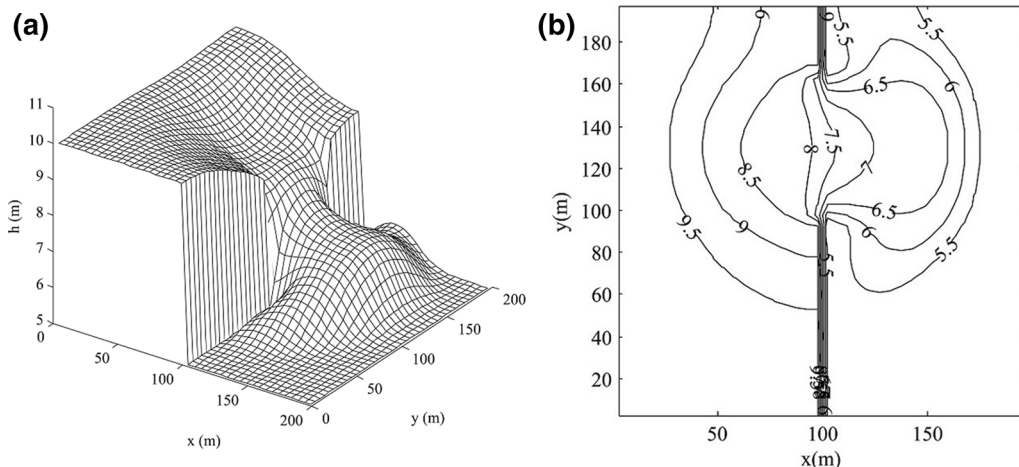


Fig. 7 The partial dam-break problem; **a** water surface elevation (m), **b** depth contours (m)

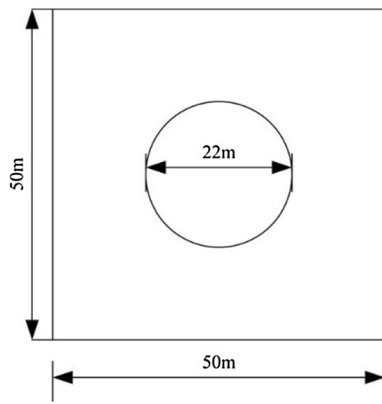


Fig. 9 The initial conditions for the circular dam-break problem

surface, water depth contours, and the velocity field at $t = 7.2$, respectively.

According to the results, the shock and rarefaction waves propagation to the right and left side of the breached dam are evidently predicted. Figure 8 depicts the velocity vectors in the flow region.

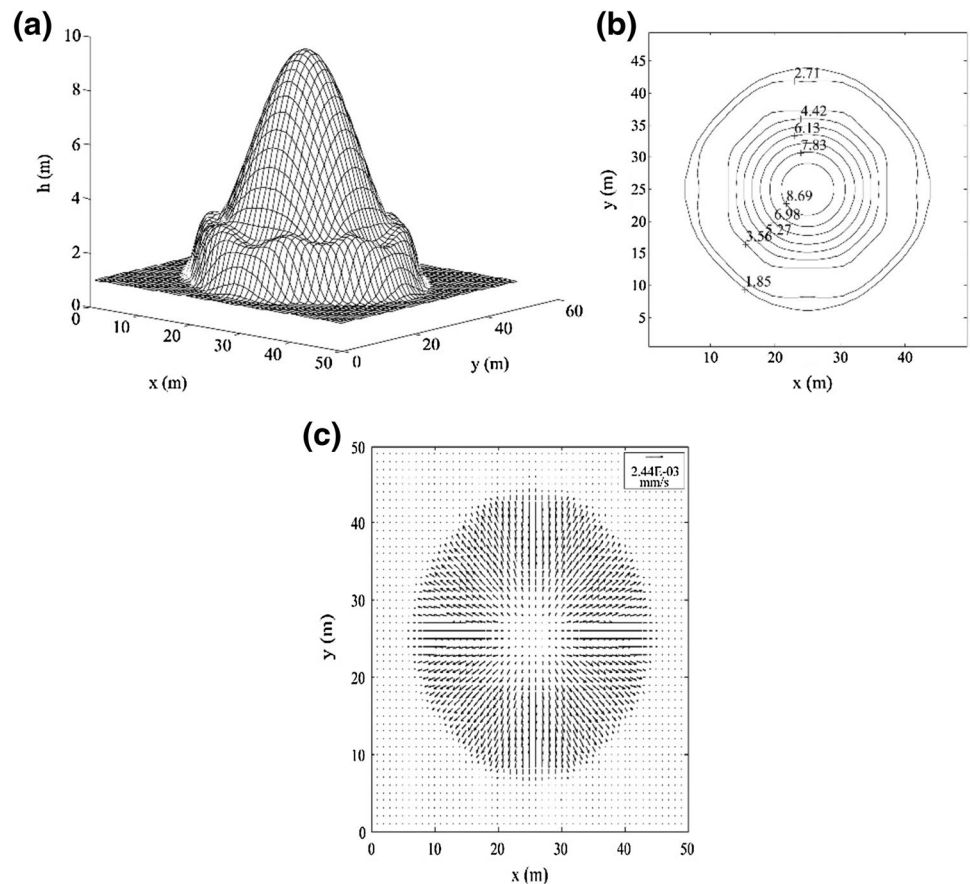
4.4 Circular dam-break problem

The developed model was also validated using the scenario of a circular dam break, as described by [33, 37, 38]. This case considers the breaking of a cylindrical dam to study the properties of the model to preserve symmetry. The initial condition is comprised of two regions of stationary water bodies, which are separated by a thin-walled cylinder of diameter 22 m located in the center of a $50 \times 50 \text{ m}^2$ horizontal and frictionless channel (Fig. 9). The domain was discretized by 5000 triangular elements. The water depth inside and outside the wall are 10 and 1 m, respectively.

Figure 10 represents the obtained depth contours and velocity vectors.

The model shows the symmetry preserving and shock-capturing characteristics. However, some variations of water depth in the form of isles are notable in Fig. 10a, b, which are the negative features of using a Cartesian coordinate system in this particular case. The model is comparable to Zachariah’s [26] solution.

Fig. 10 Circular dam-break flow using the TVD–Taylor–Galerkin method at $t = 0.69 \text{ s}$. **a** Three-dimensional view of the water elevation (m), **b** contours of water depth (m), **c** velocity field



5 Conclusions

A mixed TVD Taylor–Galerkin model was developed and applied to the shallow water equations. The performance of the model was evaluated by various benchmarks, including the one-dimensional, asymmetric, and circular dam-break flows. The following conclusions were drawn:

- The developed finite-element model has shown to act as an effective shock-capturing model.
- The model is tested to simulate both the sub- and supercritical dam-break flows with the water depth ratios of 0.5 and 0.1. Comparing the predicted results with the results of other researchers, it was noticed that the current model performs better, in terms of accuracy, especially in the supercritical flow regimes.
- Regarding the ability of the TVD-TG model to predict supercritical flows, this model can be used with some approximations to predict flows with dry beds. Accordingly, new models can be carried out by considering lower depth ratios while ignoring the corresponding source terms in the SVEs. This can result in faster calculations.
- The partial dam-break case revealed the scheme's efficiency to predict the salient features of a two-dimensional flow emanating from an asymmetric dam-break. On the other hand, the circular dam-break benchmark confirms the model's symmetry-conserving capability.

It can be seen that the combination of the TVD and Taylor–Galerkin schemes presented here can be a valuable practical tool for engineers to mitigate the spurious oscillations in the shock-dominated problems. Here, the TVD scheme operates when it is required to. Therefore, this approach can be useful in terms of time and computational costs, in order to maintain larger time steps than the CFL criterion, which can be further investigated in future works.

References

1. Lauritzen PH (2011) Numerical techniques for global atmospheric models. In: Lecture notes in computational science and engineering, vol 73. Springer, Berlin, p 572
2. Akkerman I et al (2011) Isogeometric analysis of free-surface flow. *J Comput Phys* 230:4137–4152
3. Ouyang C, He S, Xu Q (2014) MacCormack-TVD finite difference solution for dam break hydraulics over erodible sediment beds. *J Hydraul Eng* 141:06014026
4. Luo Z, Gao J (2015) The numerical simulations based on the NND finite difference scheme for shallow water wave equations including sediment concentration. *Comput Methods Appl Mech Eng* 294:245–258
5. Amini R, Maghsoodi R, Moghaddam N (2016) Simulating free surface problem using isogeometric analysis. *J Braz Soc Mech Sci Eng* 38:413–421
6. Wang P, Zhang N (2014) A large-scale wave-current coupled module with wave diffraction effect on unstructured meshes. *Sci China Phys Mech Astron* 57:1331–1342
7. Zhang M-L et al (2016) Numerical simulation of flow and bed morphology in the case of dam break floods with vegetation effect. *J Hydrodyn Ser B* 28:23–32
8. Triki A (2013) A finite element solution of the unidimensional shallow-water equation. *J Appl Mech* 80:021001
9. Ortiz P (2014) Shallow water flows over flooding areas by a flux-corrected finite element method. *J Hydraul Res* 52:241–252
10. Isakson MJ, Chotiros NP, Piper J (2015) Finite element modeling of propagation and reverberation shallow water waveguide with a variable environment. *J Acoust Soc Am* 138:1898
11. Yin J, Sun J-W, Jiao Z-F (2015) A TVD-WAF-based hybrid finite volume and finite difference scheme for nonlinearly dispersive wave equations. *Water Sci Eng* 8:239–247
12. Crespo A, Gómez-Gesteira M, Dalrymple R (2008) Modeling dam break behavior over a wet bed by a sph technique. *J Waterw Port Coast Ocean Eng* 134:313–320
13. Chang T-J et al (2011) Numerical simulation of shallow-water dam break flows in open channels using smoothed particle hydrodynamics. *J Hydrol* 408:78–90
14. Zhang M et al (2014) Integrating 1D and 2D hydrodynamic, sediment transport model for dam-break flow using finite volume method. *Sci China Phys Mech Astron* 57:774–783
15. Zarmehi F, Tavakoli A, Rahimpour M (2011) On numerical stabilization in the solution of Saint-Venant equations using the finite element method. *Comput Math Appl* 62:1957–1968
16. Atallah MH, Hazzab A (2013) A Petrov–Galerkin scheme for modeling 1D channel flow with varying width and topography. *Acta Mech* 224:707–725
17. Wang H-H et al (1972) Numerical solutions of the one-dimensional primitive equations using Galerkin approximations with localized basis functions. *Mon Weather Rev* 100:738–746
18. Sheu TWH, Fang CC (2001) High resolution finite-element analysis of shallow water equations in two dimensions. *Comput Methods Appl Mech Eng* 190:2581–2601
19. Harten A (1983) High resolution schemes for hyperbolic conservation laws. *J Comput Phys* 49:357–393
20. Wang J, Ni H, He Y (2000) Finite-difference TVD scheme for computation of dam-break problems. *J Hydraul Eng* 126:253–262
21. Boulahia A, Abboudi S, Belkhir M (2014) Simulation of viscous and reactive hypersonic flows behaviour in a shock tube facility: TVD schemes and flux limiters application. *J Appl Fluid Mech* 7:315–328
22. Ouyang C et al (2013) A MacCormack-TVD finite difference method to simulate the mass flow in mountainous terrain with variable computational domain. *Comput Geosci* 52:1–10
23. Huang Z, Lee J-J (2014) Modeling the spatial evolution of roll waves with diffusive Saint Venant equations. *J Hydraul Eng* 141:06014022
24. Vacondio R, Dal Palù A, Mignosa P (2014) GPU-enhanced finite volume shallow water solver for fast flood simulations. *Environ Model Softw* 57:60–75
25. Stoker JJ (1992) *Water waves; the mathematical theory with applications*. Pure and applied mathematics. Interscience Publishers, New York
26. Zachariah C (2000) A characteristics finite-element algorithm for computational open channel flow analysis. The University of Tennessee, Knoxville

27. Selmin V (1987) Finite element solution of hyperbolic equations II. Two dimensional case. Inria, Paris
28. Yee H, Warming R, Harten A (1983) Implicit total variation diminishing (TVD) schemes for steady-state calculations. In: 6th computational fluid dynamics conference danvers. American Institute of Aeronautics and Astronautics
29. Toro EF (2001) Shock-capturing methods for free-surface shallow flows, vol xv. Wiley, Chichester, p 309
30. Zienkiewicz OC, Taylor RL (eds) (2000) The finite element method. Butterworth-Heinemann, Oxford
31. Falconer RA (1986) Water quality simulation study of a natural harbor. *J Waterw Port Coast Ocean Eng* 112:15–34
32. Ransom O, Younis B (2015) Selective application of a total variation diminishing term to an implicit method for two-dimensional flow modelling. *J Flood Risk Manag* 8:52–61
33. Alcrudo F, Garcia-Navarro P (1993) A high-resolution Godunov-type scheme in finite volumes for the 2D shallow-water equations. *Int J Numer Meth Fluids* 16:489–505
34. Ying X, Wang S, Khan A (2003) Numerical simulation of flood inundation due to dam and levee breach. In: World water and environmental resources congress. American Society of Civil Engineers, pp 1–9
35. Liang S-J, Tang J-H, Wu M-S (2008) Solution of shallow-water equations using least-squares finite-element method. *Acta Mech Sinica* 24:523–532
36. Chou C et al (2015) Extrapolated local radial basis function collocation method for shallow water problems. *Eng Anal Bound Elem* 50:275–290
37. Neumann P, Bungartz H-J (2015) Dynamically adaptive Lattice Boltzmann simulation of shallow water flows with the Peano framework. *Appl Math Comput* 267:795–804
38. Touma R, Klingenberg C (2015) Well-balanced central finite volume methods for the Ripa system. *Appl Numer Math* 97:42–68